Atmos. Chem. Phys. Discuss., 14, 11815–11853, 2014
www.atmos-chem-phys-discuss.net/14/11815/2014/
doi:10.5194/acpd-14-11815-2014

Atmospheric Chemistry and Physics Discussions

Tropical deep convective life cycle: Cb-anvil cloud microphysics from high altitude aircraft observations

W. Frey[1,2], S. Borrmann[1,3], F. Fierli[4], R. Weigel[3], V. Mitev[5], R. Matthey[6], F. Ravegnani[4], N. M. Sitnikov[7], A. Ulanovsky[7], and F. Cairo[4]

[1]Max Planck Institute for Chemistry, Mainz, Germany
[2]School of Earth Sciences and ARC Centre of Excellence for Climate System Science, University of Melbourne, Melbourne, Australia
[3]Institute for Atmospheric Physics, Johannes Gutenberg University, Mainz, Germany
[4]Institute of Atmospheric Science and Climate, ISAC-CNR, Rome, Italy
[5]Swiss Centre for Electronics and Microtechnology, Neuchâtel, Switzerland
[6]Dept. of Science, University of Neuchâtel, Neuchâtel, Switzerland
[7]Central Aerological Observatory, Dolgoprudny, Moscow Region, Russia

Received: 24 April 2014 – Accepted: 30 April 2014 – Published: 12 May 2014

Correspondence to: W. Frey (wiebke.frey@unimelb.edu.au)

Published by Copernicus Publications on behalf of the European Geosciences Union.

Abstract

The case study presented here focusses on the life cycle of clouds in a tropical deep convective system. During the SCOUT-O3 campaign from Darwin, Northern Australia, the Hector storm system has been probed by the Geophysica high altitude aircraft. Clouds were observed by in situ particle probes, a backscatter sonde, and a miniature lidar. Additionally, aerosol number concentrations have been measured. On 30 November 2005 a double flight took place and Hector was probed throughout its life cycle in its developing, mature, and dissipating stage. The two flights were four hours apart and focussed on the anvil region of Hector in altitudes between 10.5 km and 18.8 km (i.e. above 350 K potential temperature). Trajectory calculations and ozone measurements have been used to identify that the same cloud air masses have been probed in both flights.

The size distributions derived from the measurements not only show a change with increasing altitude but also with the evolution of Hector. Clearly different aerosol to cloud particle ratios as well as varying ice crystal morphology have been found for the different development stages of Hector, indicating a change in freezing mechanisms. The development phase exhibits the smallest ice particles (up to 300 µm) with a rather uniform morphology. This is indicative for rapid glaciation during Hector's development. Sizes of ice crystals are largest in the mature stage (larger 1.6 mm) and even exceed those of some continental tropical deep convective clouds, also in their number concentrations. The backscatter properties and particle images show a change from frozen droplets in the developing phase to rimed and aggregated particles. The clouds in the dissipating stage have a large vertical ~~extend~~ (roughly 6 km) though optically thin and persist for at least 6 h. This poses a high potential for affecting the tropical tropopause layer background conditions regarding humidity, e.g. through facilitating subvisible cirrus formation, and with this the amount of water vapour that is transported into the stratosphere.

1 Introduction

Deep convection provides a fast pathway to transport air masses from the boundary layer to the free troposphere, sometimes reaching the tropopause region or overshooting even above (Fueglistaler et al., 2009). Thus, trace gases, water vapour, and aerosols are redistributed effectively in the atmosphere. Clouds form in this convective environment and may build large cloud shields, which have an important impact on the radiation balance, regulating incoming solar and outgoing longwave radiation (Baker, 1997; Baker and Peter, 2008). Ice crystals in the clouds provide surfaces for heterogeneous chemical reactions which may contribute to ozone destruction (e.g. Borrmann et al., 1996; Solomon et al., 1997; von Hobe et al., 2011), also in the tropics. Furthermore, water and condensable gases are removed from the gas phase by adsorption onto the cloud particles and thus depleted from the air masses and aerosols can be washed out by cloud particles. In what manner clouds impact climate and chemistry critically depends on their microphysics, i.e. sizes and numbers of cloud particles, as well as ice crystal shapes (Lynch, 2002). Furthermore, the microphysics determine the amount of water vapour that is transported from the tropical troposphere to the stratosphere (Winker and Trepte, 1998; Corti et al., 2008; Jensen et al., 2008; de Reus et al., 2009; Davis et al., 2010), where it plays a central role in radiative and chemical processes. Additionally, in order to realistically represent the tropical high altitude clouds in numerical models and to test the model output one needs to know the cloud microphysical structure. Knowledge of these properties can only be obtained by in situ measurements. Despite the amount of cloud observations from satellite or ground based instruments, those observations are unable to resolve the microphysical structures. Thus, little is known about the microphysical properties of cirrus clouds, particularly at high altitudes in the tropics, due to the lack of in situ measurements.

In the tropics, the transition from troposphere to stratosphere occurs in a transition layer rather than at a sharp boundary. This Tropical Tropopause Layer (TTL) is usually defined at altitudes between 14–18 km and it is the dominant source region of air en-

tering the stratosphere (Park et al., 2007; Fueglistaler et al., 2009). The level of zero radiative heating and the cold point tropopause are located within the TTL. Residence times for air parcels in the TTL are roughly two months (Krüger et al., 2009). Thus, the dynamical and radiative characteristics of the TTL allow microphysical and chemical processes to affect tropospheric air entering the stratosphere to a great extent. Furthermore, the lowest TTL altitude levels have been identified as a region where frequent new particle formation events occur in clear air as well as in cumulonimbus cloud anvils (Weigel et al., 2011; Frey et al., 2011) with unknown consequences for the aerosol in the lower stratosphere. Direct measurements of the microphysical properties of tropical deep convective clouds close to the convective core in the TTL can only be obtained by highly specialised high altitude research aircraft in these regions (e.g. McFarquhar and Heymsfield, 1997; de Reus et al., 2009; Frey et al., 2011). Satellite and ground based remote sensing on the other hand are not able to obtain observations of microphysical properties. Other in situ studies were performed using aircraft not reaching the TTL. Furthermore, previous studies involving aircraft often focussed only on the development and mature stages of tropical convection, or even just on parts of the convective clouds, e.g. convective overshooting, but little attention has been paid to the dissipating stage. So the question remains how the microphysical properties of convective clouds in the tropical tropopause layer look like, especially throughout their lifetime.

Modelling efforts often look at the more general structure of convective clouds and are not dealing with detailed microphysics due to its heavy numerical burden. As for the observational studies, the interest of numerical experiments is mostly focussed on the developing and mature stages of a convective cell, as well as on convective overshooting, but rarely touches the dissipating stage and thus not the complete life cycle of the clouds. For example, Saito et al. (2001) simulated the diurnal evolution of a Hector thunderstorm (Keenan et al., 1994; Carbone et al., 2000). This deep convective system, which can be found over the Tiwi Islands, Northern Australia, makes nearby Darwin with its scientific infrastructure a natural laboratory for studies of deep convection (Brunner

et al., 2009). Saito et al. (2001) point out the sensitivity of the storm development to ice phase physics and island-scale circulations, however, when coming to the dissipating stage they state: "Since the decay of convection is not the primary interest, it is not examined further." Other reasons for not looking into the decaying state may be due to models failing to predict the dissipating stage correctly. Chemel et al. (2009) mentioned a dramatically different structure of the TTL after Hector in simulations of the Advanced Research Weather Research and Forecasting (WRF) and the Met Office Unified Model (UM) models, indicating that the dissipating stage is not well represented in at least one of the models. Connolly et al. (2013) suggest that microphysics schemes may produce anvils which have a too small extent and persistence due to the assumed density of snow. However, the decay of a deep convective system may have major implications for the formation of subvisible cirrus (SVC), by affecting the background conditions e.g. regarding humidity. These cirrus can occur in widespread layers, though vertically only reaching a few 100 m, close to the tropical cold point tropopause (Winker and Trepte, 1998). Their importance for radiative effects and dehydration of tropopause air which is further transported into the stratosphere is a point of discussion (Rosenfield et al., 1998; Corti et al., 2006; Davis et al., 2010). SVC can either be formed in situ or due to blow-off from deep convection. E.g. Massie et al. (2002) found that half of the SVC observations by the Halogen Occultation Experiment (HALOE) over the maritime continent are consistent with formation via convective blow-off. This picture may vary from region to region: using Global Hawk observations, Jensen et al. (2013) concluded that most likely SVC over the east Pacific have formed in situ. However, this region is in general less convectively active than the maritime continent. Jensen et al. (1996) studied the formation mechanisms of SVC and simulated convectively formed SVC. They point out the role of wind shear on convective blow-off for formation of cloud layers with vertical thicknesses less than 1 km. Thus, gaining more insight of the dissipating stage of deep convective systems, will also be helpful for understanding SVC formation, either from remnants of convection or facilitated through the changed background conditions. Also, after the dissipation of large cloud systems, like Hector, patches of

"left over clouds" and of enhanced numbers of larger, swollen, humidified aerosol particles still may remain in the air mass of the original deep convective cloud. The radiative effects of this air, which is not yet completely cloud free, will be different from clear air and from cloudy air resembling more the "twilight zone" brought forward by Koren et al. (2007). For these reasons closer consideration of the dissipation stages of cloud systems is important from the perspective of the radiative budget and also of the satellite data retrieval and analyses.

This work is a case study using in situ observations of a Hector thunderstorm obtained during ~~a double flight~~ on 30 November 2005 in order to document and provide data about the microphysical properties of a deep convective cloud in the TTL throughout its life cycle.

2 Experiment and instrumentation

2.1 SCOUT-O3 campaign

As part of the European integrated project Stratospheric–Climate Links with Emphasis on the Upper Troposphere and Lower Stratosphere (SCOUT-O3; Brunner et al., 2009) an aircraft campaign was conducted from Darwin, Northern Australia in November/December 2005. The main objectives of this campaign were to investigate the transport and transformation of trace gases, water vapour, and aerosols through the TTL and the role of deep convection therein. Darwin was chosen as base for the experiment due to its vicinity to the Tiwi Islands and the Hector storm system which develops on an almost daily basis during premonsoon season above those islands. ~~Mostly~~ Hector develops ~~as~~ a consequence of an interaction between sea breeze fronts and convectively generated cold pools above the islands (Carbone et al., 2000). The aircraft probing the air masses over and in the vicinity of the Tiwi Islands and the Hector system was the Russian M55 "Geophysica" high altitude research aircraft with a ceiling of 20 km. The Geophysica performed nine flights with different foci, i.e. studying

convection, long range transport, and perform satellite validation. Brunner et al. (2009) describe the large scale meteorological context of the campaign, details of the meteorological context for this study can be found in Sect. 3.

2.1.1 ~~Cloud particle~~ instrumentation

Two instruments were used to observe cloud particles: a modified Particle Measuring Systems (PMS) Forward Scattering Spectrometer Probe (FSSP-100) with Droplet Measurement Technologies (DMT) high speed electronics (SPP-100) and a DMT Cloud Imaging Probe (CIP). The instruments cover a size range (in diameter D_p) of 2.7 µm < D_p < 29.2 µm (FSSP-100) and 25 µm < D_p < 1600 µm with a 25 µm resolution (CIP). The characteristics of both instruments are described in de Reus et al. (2009) and Frey et al. (2011, and references therein). Since the FSSP-100 sampled data in a 2 s interval, the CIP data have been averaged over 2 s as well in order to combine with the FSSP-100 measurements. The uncertainties of the measured number concentrations are mainly determined by the uncertainties in the sample volumes, which were estimated to be 20 % (Baumgardner et al., 1992; de Reus et al., 2009) for both probes. Additional uncertainty due to counting statistics has been taken into account especially in conditions with low particle number concentrations. For the calculation of size distributions integration times have been adequately extended, depending on the particular conditions of each measurement period during the flight. The cloud particle data have been thoroughly filtered for shattering artefacts, following the interarrival time approach (Field et al., 2006), since the probe came with the original tips (i.e. not anti shattering optimised). Furthermore, as shown by de Reus et al. (2009) and Cairo et al. (2011), who used comparisons of the cloud particle data from CIP and FSSP to lyman-alpha hygrometers and a backscatter sonde respectively, shattering was not a problem for these particular samplings of Hector clouds. A further set of corrections has been applied to the CIP images, i.e. accounting for the loss of the first slice (due to slow acquisition start-up time), empty images (reconstructed as one pixel image), partial images, out of focus images, airspeed, and too small area ratio (rejection of streakers). A detailed description of these corrections and the capability of the instruments to measure reliably under the conditions in the upper troposphere and lower stratosphere can be found in Frey et al. (2011, and the accompanying supplement material, which also includes an extensive discussion of possible shattering artefacts).

Further cloud properties were measured by the Multiwavelength Aerosol Scatterometer (MAS; Cairo et al., 2004; Buontempo et al., 2006). This backscatter sonde obtains in situ measurements of optical properties and microphysical parameters of aerosol and cloud particles, e.g. backscatter ratio and aerosol depolarisation (at 532 nm and 1064 nm). MAS samples with a time resolution of 5 s and has a precision of 10 %. The downward looking Miniature Aerosol Lidar (MAL; Mitev et al., 2002) detects vertical profiles of aerosol and cloud particles below the aircraft, as close as 160 m from the aircraft. MAL measures with 60 s horizontal integration and 43 m vertical resolution.

2.2 Further instrumentation

Aerosol number concentrations were measured with 1 Hz resolution and with 10 % accuracy by two COndensation PArticle counting Systems (COPAS; Curtius et al., 2005; Weigel et al., 2009), consisting of four Condensation Particle Counter (CPC) channels. The 50 %-detection efficiency size (D_{p50}) for these channels are at particle diameters of 6 nm, 10 nm, and 15 nm (number concentrations denoted as N_6, N_{10}, and N_{15}), respectively, and the fourth CPC channel (D_{p50} = 10 nm, N_{10nv}) is preheated to 250 °C in order to evaporate volatile compounds and detect ~~possibly occurring~~ non-volatile residues.

Ambient and potential temperature have been measured by the Thermo Dynamic Complex (TDC) probe at 1 Hz with an accuracy of 0.5 K (Shur et al., 2007). The navigational system UCSE (Unit for Connection with the Scientific Equipment; Sokolov and Lepuchov, 1998) aboard the Geophysica delivered further relevant parameters as position and true air speed.

The FLourescent Airborne Stratospheric Hygrometer (FLASH; Khaykin et al., 2009; Sitnikov et al., 2007) was adopted to measure gas phase water, sampling at 1 Hz. The

accuracy is 8 % or 0.3 ppmv, and combined with the TDC temperature measurements the uncertainty of relative humidity with respect to ice is 12–17 %.

The Fast OZone ANalyzer (FOZAN; Yushkov et al., 1999; Ulanovsky et al., 2001) measured ozone mixing ratios at 1 Hz sampling frequency. It is a chemiluminescence sensor with an accuracy of 10 % and a precision of 0.01 ppm.

3 30 November 2005 – description of the case

A strong Hector storm system developed on 30 November 2005 over the Tiwi Islands north of Darwin, Australia. On this day two research flights have been carried out. The first flight (about 03:45 UTC to 08:20 UTC/13:15 LT to 17:50 LT) probed Hector during its developing and mature ~~stage~~ while the second flight (about 12:10 UTC to 17:30 UTC/21:40 LT to 03:00 LT next day) probed Hector in its dissipating stage, with roughly 4.5 hours of sampling time inside the upper parts of Hector. Due to flight safety, the Geophysica did not fly in the convective core itself, but above and around the strong up- and downdrafts, thus, on top of Hector and within the anvil clouds. During the first flight overshooting cloud tops have been penetrated in altitudes up to 18.7 km (Corti et al., 2008; de Reus et al., 2009), with lowest cloud top temperatures below 190 K. The cold point tropopause was situated at around 17.3 km and had a temperature of 185.5 K. The meteorological development of this particular Hector to its mature stage is described in detail by Chemel et al. (2009) making use of cloud resolving modelling, albeit without including information on microphysical properties of the clouds. They used the WRF and the UM models with horizontal resolutions of 1 km and with this were able to reproduce the overshooting cloud turrets. These overshoots lead to troposphere–stratosphere exchanges, in particular affecting the entry of water vapour in the lower stratosphere. They found a fairly significant moistening above the 380 K isentrope (on average 0.06 ppmv (WRF)/2.24 ppmv (UM) between 380 and 420 K), while Corti et al. (2008) found positive deviations from measured mean water vapour profiles of up to 1.4 ppmv.

Satellite imagery in the infra red (IR) for cloud top temperatures is available from the Geostationary Meteorological Satellite 5 (GMS-5), operated by the Japan Meteorological Agency. Figure 1 shows a single GMS satellite image at 03:33 UTC/13:03 LT where the first cloud patches of Hector can be seen over the Tiwi Islands. The coloured lines show the contours of Hector during its development: blue at 04:33 UTC, green at 05:33 UTC, and red at 06:33 UTC. These contours were fitted to the coloured pixels of the respective satellite images. The white contour gives an estimate of the maximum extension of Hector derived from the satellite image at 10:33 UTC/20:03 LT, where Hector already started to dissolve. The figure shows that Hector spread out over the Tiwi islands with its ~~position~~ remaining stationary during the time span covered by the two Geophysica flights on that day. The ~~dissolving~~ of Hector is depicted in Fig. 2, which shows the satellite images of 09:33, 10:33, and 11:33 UTC (19:03, 20:03, and 21:03 LT). While the IR satellite images clearly show the presence of clouds with very high optical thicknesses $\tau \geq 100$ (MTSAT IR NASA LARC cloud product: http://cloudsgate2.larc.nasa.gov/cgi-bin/site/showdoc?docid=22&domain=mtsat&lkdomain=Y) during the first flight on 30 November, the IR satellite images of the second flight ~~almost show~~ no clouds and optical thicknesses are at maximum 2. However, extensive cloud fields have been probed by the aircraft also during the second flight as evident from the measurements ~~of~~ the in situ cloud particle instrumentation as well as the backscatter sonde and miniature lidar. The latter clearly shows the existence of ice clouds, inferred from depolarisation measurements (volume depolarisation ration = signal in depolarisation channel/signal in parallel-polarisation channel), as evident from Fig. 3. In those lidar measurements a return from the surface has always been detected, suggesting a cloud optical thickness not exceeding 3. Apparently after the Hector encounter during the first flight, some clouds remained in place at around 10–16 km altitude. After these considerations we believe the cloud was not optically thick enough anymore to give sufficient signal for the satellite sensor.

The fact that Hector stayed in place during its development (compare Figs. 1 and 2) leads to the assumption that during the first and second flight the same air masses

have been probed. Figure 4 shows the wind fields on the 100 hPa and 200 hPa levels (roughly reflecting flight altitude) on 30 November 2005 at 06:00 and 12:00 UTC (15:30 and 21:30 LT). Wind speeds around the Tiwi Islands were generally low, so there was no large scale transport of air masses on this day. Ten day backtrajectories are calculated from ECMWF fields at 0.5° resolution with a kinematic code on a 0.2° × 0.2° 3-D box surrounding the flight path. The closest starting point (in space, time, and height) is attributed to each point of the flight path. These backtrajectories, starting along the tracks of the first and second flight, show a general flow from Southeast Asia (Philippines) to the Indian Ocean and then turning towards Australia where they finally reach the Tiwi Islands as a south westerly flow. In order to identify whether air masses sampled during the second flight were coming from the area of the first flight, six hours synoptic backtrajectories originating from the second flight were calculated. These trajectories indicate that the winds between the two flights were weak and air parcels recirculated in the area after being advected to the islands from south-east. A west-east jet was located in the south of the Islands, which did not extend to the measurement region. On the contrary, the area covered by the Geophysica above the Tiwi Islands was located in a relatively quiet zone to the North of the jet.

Furthermore, measurements of ozone mixing ratios have been taken into account in order to check for air mass exchange. Figure 5 shows the observed ozone profiles of the first and second flight. The left hand side shows the individual data points, the right hand side the median and 33/67 percentiles. The profiles agree well in the middle troposphere (353–350 K potential temperature) while they differ by up 26 ppbv in the TTL region. This difference can be attributed to upward mixing of low ozone mixing ratios from the boundary layer (Solomon et al., 2005). This is corroborated by noting from the right panel of Fig. 5 that the same low ozone values (about 40 ppbv at 300 K potential temperature; dark blue) from flight 1 appear during flight 2 between 365 and 375 K (light blue). Air masses in deep convection can be transported from the lower troposphere into the upper troposphere in about 30 min (Thompson et al., 1997). Thus, given the lifetime of ozone in the TTL, a signature of this upward transport can be

expected, if no advection of undisturbed air masses from the side takes place. The higher ozone values of the data points enclosed by the orange ellipse were sampled in cloud free air and at the cloud edge upwind of the Hector anvil and its convective core. Thus, the ozone reduction due to upward transport of low level air did not take place here, also keeping in mind that the flow was coming from the East.

Taking the satellite images and the trajectories for the two flights on 30 November it seems reasonable to assume that the same air mass had been probed twice and that replacement of the air mass probed during the first flight with more recently advected different air did not occur here.

4 Microphysical evolution of Hector

4.1 Observations of size distributions in Hector development stages

During the double flight clouds were penetrated by the aircraft and a set of size distributions was measured. The cloud measurements of both flights were collected and separated into the following groups: developing Hector, overshoots, mature Hector, and dissolving Hector. Measurements obtained between take off of the first flight (03:44 UTC) and 04:47 UTC/14:17 LT are classified as developing Hector. Between 04:47 UTC and 07:00 UTC/16:30 LT clouds have been probed in convective overshooting regions in the stratosphere. The analyses of these measurements are described in detail by de Reus et al. (2009) and Corti et al. (2008) and are not further considered here, because of their focus on higher altitudes. Size distributions observed between 07:00 UTC and landing (08:18 UTC/17:48 LT) are classified as mature Hector. All size distribution from the second flight (12:19–17:21 UTC/21:49–02:51 LT) fall into the dissolving Hector class (however, cloud measurements were only analysed until 15:30 UTC/01:00 LT, due to an FSSP-100 power failure afterwards). The dissolving Hector size distributions have further been checked and filtered for possible influence of non-Hector clouds on the southern flight part, according to the 6 h backtrajectories on the flightpath of the sec-

ond flight. When the trajectories indicated a possible influence of a non-Hector cloud, the size distribution was excluded from the analysis. This resulted in the loss of roughly a third of the size distributions in the dissipating stage. The Hector size distributions are then classified into altitude bins of 5 K potential temperature. The vertical profile of the averages of every class are shown in Fig. 6. Most size distributions are averaged over a sample time period of 20–25 s (corresponding to roughly 3–5 km flight path), in case of small number concentrations this averaging time is extended to up to 145 s (about 25 km flight distance) in order to obtain better sampling statistics. The numbers (#) of compiled size distributions per class and potential temperature bin are given in Table 1 together with mean values for ice water content (IWC), number concentrations (N), effective radius (r_{eff}), relative humidity with respect to ice (RHi), and ambient temperature (T). The general findings from Fig. 6 are as follows:

- The size distributions show a decrease in number concentrations and particle size with increasing altitude. This has also been observed by Frey et al. (2011) and de Reus et al. (2009). The only exception is the developing case that exhibits clearly higher number concentrations in the 365–370 K bin, contrary to the general decrease in number concentrations with altitude.
- The mature ~~Hector~~ exhibits the largest number concentrations and sizes, as expected, while the smallest particle sizes and concentrations can be found for the developing Hector cases. Exception: in the 365–370 K-bin number concentrations for the small particles are largest for the developing ~~Hector case~~.
- Table 1 shows that the mature ~~Hector~~ stages exhibit the largest values for the microphysical parameters in each altitude bin, followed by the dissipating stage and the developing stage having smallest values. There are two exceptions: in the 355–360 K bin the effective radius of the developing Hector stage is slightly larger than the dissipating stage and in the 365–370 K bin the developing ~~Hector~~ has higher number concentrations than the dissipating stage, almost as high as those for the mature stage.

- The ambient temperature became warmer with increasing age of Hector. (The only exception here is the dissipating Hector stage in the 365–370 K bin, however, only one size distribution is given here, which was sampled over 60 s.)
- In the highest altitude bin the size distributions for all cases are fairly similar, only differing in the sizes of the largest detected particles.

4.2 Comparison with data from West African Mesoscale Convective Systems

The thin black lines in Fig. 6 show the median size distributions of clouds measured in the vicinity of West African Mesoscale Convective Systems (MCS) during the SCOUT-AMMA campaign (Frey et al., 2011) for comparison. These MCS are correlated to African Easterly Waves and further triggered by topographic features (Mekonnen et al., 2006). While the size distributions of the AMMA clouds and the ~~mature Hector~~ look very similar in the 350–355 K bin, the mature ~~Hector~~ exhibits much larger and more cloud particles in the altitude range from 355 K to 370 K. In these altitudes the AMMA clouds compare fairly well to the developing and dissipating Hector clouds, despite some small differences: (a) in the 355–360 K range the cloud particles during AMMA have a smaller maximum diameter (up to 100 µm compared to 300 µm/250 µm); (b) in the 360–365 K bin the developing Hector has smaller ice crystals than the AMMA clouds, while the dissolving Hector shows a larger amount of small particles than the AMMA clouds; (c) in the 365–370 K range the dissolving Hector compares well to the AMMA clouds, while the developing Hector has more than an order of magnitude more smaller particles. Thus interestingly, this case study points out the possibility of Hector to create larger ice crystals than continental Mesoscale Convective Systems over West Africa (Frey et al., 2011), even though continental convection is generally thought to produce stronger updrafts and with this larger hydrometeors (Cetrone and Houze, 2009; Frey et al., 2011). Of course in all these considerations it has to be noted that the size distributions here display the median for the West African MCS and thus single clouds may show more and larger cloud particles. On the other hand, the Hector observa-

tions here display only one case study and this Hector was a very strong one, even overshooting into the stratosphere (Corti et al., 2008; de Reus et al., 2009). Though it seems perspicuous to look at the convective available potential energy (CAPE) in order to compare the convective strength of the MCS and Hector, Carbone et al. (2000) point out that CAPE in Hector may vary considerably and is weakly correlated with convective strength. Nevertheless, the observations presented here clearly reveal the potential of Hector to produce very large hydrometeors comparable to or even larger than those in continental convection.

4.3 Potential for SVC generation

The size distributions, particularly of the dissipating Hector stages, in the upper two bins of Fig. 6 show a similarity to subvisible cirrus (SVC, Davis et al., 2010; Frey et al., 2011). Frey et al. (2011) ~~comprised~~ all reported SVC measurements into one fit function which is displayed here in grey, the shading denotes the standard deviation from the fit function. It can be excluded that the clouds in the different Hector stages are SVC: the geometrical thickness is much larger than that of a typical SVC, i.e. more than 6 km vertical extension in the dissipating stage compared to less than 1 km for SVC. Furthermore, the developing and mature cases are directly linked to the convective storm and are also optically too thick, as can clearly be inferred from satellite images. However, this illustration shows that the dissipating Hector might be a precursor for SVC: the upper cloud part may persist~~s~~ while the lower cloud parts diminish or wind shear may split the cloud into thin ~~cloud~~ layers (Jensen et al., 1996) and thus transform parts of this cloud layer into SVC. On the other hand, if this layer dissipates completely after some more time, it will leave behind a layer of humidified air in the TTL which might be favourable for SVC formation. Even if not dissipating further and/or ~~transform~~ into a SVC, the cloud may take up more humidity causing ice particles to grow, sediment, and dehydrate the air. Since air in this region is subject to slow upwelling, changes in humidity here impact the stratospheric humidity.

5 Backscatter and aerosol measurements and their implication for freezing history

More information about the clouds and their structure can be obtained from the backscattersonde MAS optical measurements. Figure 7 shows profiles of aerosol backscatter coefficient and aerosol depolarisation for the cloud cases and bins as in Fig. 6. Only in-cloud data are presented. The aerosol backscatter coefficient on the left demonstrates the expected, namely that the largest backscattering occurs in the mature ~~Hector case~~, while the smallest occur in the developing ~~Hector~~. The altitude of the maximum of the backscattering on the profiles descends as time evolves. The maximum in the developing/mature/dissipating stage lies in the 365–370 K/355–365 K/355–360 K ~~bin~~, respectively. This behaviour agrees with the observed distributions of cloud particle surface density (as derived from the particle probe observations but not shown here) and with the maxima seen in the size distribution plot in the smaller ice particle size range (up to about 20 µm) for each development class. The aerosol depolarisation (right panel) is more or less constant in the developing ~~Hector case~~ and decreasing with altitude for the mature and dissipating ~~Hector~~ stages. Thus, glaciation had already taken place before the observations in the developing ~~Hector~~ (all cases at $T < 200$ K), which judging from the satellite pictures was in it's first hour of development. Therefore, there is no altitude variation. On the other side, the decreasing levels of depolarisation with altitude for the mature and dissipating Hector case, that reflects a change in the average morphology of the particles, suggests an increasing role for the gravitational settling, riming and growth by accretion. This is also confirmed by colour index measurements (not shown) which show how the largest particles were present in the lower parts of the cloud. ~~Heymsfield et al. (2005) and Heymsfield et al. (2009)~~ showed that in convective cells with strong updrafts supercooled cloud droplets reach the homogeneous nucleation level (at about −38 °C) and rapidly freeze there. Those smaller newly frozen ice crystals are transported further upwards in the convective core during the development stage without much riming. Whereas in the mature stage also larger par-

ticles reach the upper parts of the cloud. Those larger crystals are a result of riming and aggregation in the mixed phase part of the cloud at lower levels, or aggregation due to electrical charges (Stith et al., 2004).

In order to shed light on aerosol cloud interactions, and possibly gaining information about the freezing history of the cloud, one can look at the correlation between aerosol and cloud particle number concentrations. Furthermore, if assuming that aerosol and cloud particles are transported with the same efficiency in the convective updrafts then this relation can also be used to estimate how effectively aerosol particles are activated to cloud particles. In this regard, the cloud particle number concentrations would be used as a proxy for the residual aerosol (i.e. activated aerosol) particles, while the COPAS N_{15} measurements represent a proxy for the interstitial aerosol. Since the COPAS inlet does not aspirate particles larger than 1 µm with proper efficiency and aerosol number concentrations are much larger than the cloud number concentrations, the contribution of possibly counted cloud particles in the COPAS system are negligible. However, it has to be noted that due to flight safety the Geophysica did not fly in the region of strong up- and downdrafts but either above or in the outflow region around it. Thus, some effects of further processing might apply to this estimate. Figure 8 shows the aerosol number concentrations vs. cloud particle number concentrations for the selected Hector cases. $N_{aerosol}$ refers to the COPAS N_{15} measurements in most cases, in some of the ~~dissolving~~ Hector cases N_{10} have been used instead, since N_{15} measurements were not available. However, cloud segments where new particle formation events occurred (as observed by Weigel et al., 2011) were identified and excluded from the analysis here. New particle formation events are not thought to enhance the N_{15} significantly since the newly formed particles are smaller than 15 nm. The coloured symbols represent the different Hector stages: light blue dots represent developing ~~Hector~~, mature ~~Hector~~ cases are depicted by red squares, overshooting cases are shown in dark blue triangles, and the dissipating stage of Hector is displayed by green stars. The developing ~~Hector~~ cases all group very closely together, though the observations were located at very different altitudes. This is in good agreement with the

depolarisation ratio profile in Fig. 7, which remains almost constant with respect to altitude. Both findings suggests that these cloud parts were formed under very similar conditions and underwent the same freezing mechanism within a short time. There is one outlier in the developing Hector cases with lower aerosol and cloud particle concentrations, which corresponds to the size distribution in the highest altitude bin. Possibly the updraft was weakened when reaching this altitude, and thus not transporting as much of the newly frozen small cloud particles as to the other altitudes. The mature ~~Hector~~ cases have similar amount of aerosol particles, but a much higher amount of cloud particles than the developing cases. The cloud particles in this stage have undergone some riming and aggregation, thus larger ice crystals were formed. Examples for recorded particle images of such rimed and aggregated crystals are shown in Fig. 9. This change is reflected in the size distributions in Fig. 6, showing an increase in the total particle number, as well as in the higher backscatter depicted in Fig. 7. Ice multiplication processes as rime splintering (Hallett and Mossop, 1974) during the riming might be the reason for higher cloud particle concentrations while aerosol concentrations stay fairly similar to those of the developing Hector cases. Also here, there are some outliers on the side of lower aerosol and cloud particle concentrations, which correspond to size distributions in the higher altitude bins. Compared to the other Hector stages, the dissipating ~~Hector~~ cases show the largest spread in the data points. This might be an effect of ageing of the clouds, where in the course of time aerosol particles are collected on the cloud particle surfaces but on the other side might be released when particles (partly) evaporate. Examples of particle images for the dissipating stage are also given in Fig. 9. To complete the picture, the overshooting events are displayed as well. They exhibit fairly high cloud particle concentrations but less aerosol than the developing and mature cases. In these cases aerosol number concentrations are higher than the stratospheric background (on this day 20–40 cm^{-3}) and are comparable to upper tropospheric values. This is an indication that not only cloud particles but also aerosol particles were transported upwards into the stratosphere by the overshooting convection.

Figure 8 additionally shows some correlation lines, e.g. the 1 : 3000 line denotes where one out of 3000 aerosol particles would be activated to a cloud particle, under the above mentioned assumptions. It can be seen that the developing Hector cases have in general the smallest aerosol to cloud particle ratio compared to the other cases, while the mature and overshooting events exhibit the highest ratios. This is also obvious in Table 2, which summarises the averages for activation ratio estimate and aerosol number concentrations. The fast updrafts in the developing stage of Hector may lead to rapid glaciation of supercooled water (e.g. observed in Keenan et al., 1994; Heymsfield et al., 2005), thus, the grouping of the data points and the rather low aerosol to cloud particle ratio can be a hint for homogeneous freezing/rapid glaciation in such updraft. Higher aerosol to cloud particle ratios can either be an effect of different freezing mechanisms, e.g. involving contact freezing, or occur due to washout effects. The again lower ratios during the ~~dissolving~~ stage of Hector could be explained by evaporation and subsequent release of ice nuclei and other aerosol particles which had been collected onto the cloud particle surface. Even though events of new particle formation have been excluded from the analysis, it cannot be ruled out completely that during such events particles have already grown to sizes larger than 15 nm. Those particles could deliver an additional source for aerosol particles that reduce the aerosol to cloud particle ratio. However, such effects were very local and could, as an estimate, extend over about 5 km. In general, there is a decrease in cloud to aerosol particle ratio in the mature and dissipating Hector stages while the ratio is fairly constant in the developing stage (see Table 2). There are two exceptions for the cloud particle number concentration maxima in the developing case (365–370 K) and mature case (360–365 K).

It is well known that aerosols are important for cloud development. Allen et al. (2008) provided measurements of the aerosol concentrations in the background conditions of the boundary layer in the pre-monsoon and monsoon period over the Tiwi Islands. Using those observed number concentrations Connolly et al. (2013) have shown that the observed Hector storm systems were indeed influenced by the aerosol number concentrations and that by taking those into account the simulations were mostly improved,

e.g. by changing the formation and strength of Hector. Since the data presented here were obtained in the TTL region, they cannot be used for model initialisation. However, they can be used for model evaluation and testing the robustness of the treatment of aerosol-cloud-interactions in the cloud microphysics schemes. Thus, the data here complement the measurements of Allen et al. (2008).

6 Conclusions

This case study presents in situ measurements of cloud microphyiscal properties of a Hector thunderstorm. Due to the double flight it was possible to obtain measurements throughout a large part of the life cycle of Hector~~, which would not have been possible with just a single flight~~. This gave us the unique opportunity to classify the size distributions in terms of cloud development stages, a net advantage with respect to other former studies that looked at size distributions in tropical deep convective clouds (e.g. McFarquhar and Heymsfield, 1997; de Reus et al., 2009). ~~As mentioned in the introduction, m~~ost experimental as well as modelling work ~~focussed~~ on the developing and mature stages of Hector but not on its dissipating stage~~, due to various reasons~~. However, as shown here the dissipating stage exhibits a vertically extensive cloud layer of roughly 6 km, spread out through the TTL.

The data are classified into developing, mature, and ~~dissolving Hector~~ stages and additionally into altitude bins of 5 K potential temperature. The evolution of the particle properties with time and altitude is shown. The developing ~~Hector~~ stage exhibits rather small ice particles (maximum size 300 µm) compared to the later ~~development~~ stages. Maximum particle sizes are seen in the mature ~~Hector~~ cases (larger than 1 mm), even exceeding sizes of continental tropical convection. Furthermore, the mature stage exhibits the largest number concentrations as well as ice water content and effective radii. The developing cases show the lowest number concentrations, ice water contents and smallest effective radii, except in the altitude between 365–370 K, where number

concentrations and effective ~~radius~~ exceed those of the dissipating Hector cases. The values for the microphysical parameters are summarised in Table 1.

The development of the Hector clouds is also obvious in the aerosol to cloud particle ratio. Furthermore it gives indications for a change in freezing mechanisms with increasing time of Hector: the developing Hector shows very similar aerosol to cloud particle ratios and cloud particle morphology, indicating a rapid freezing under similar conditions, as homogeneous freezing. The mature Hector cases show rimed ice crystals and some chain aggregates, higher aerosol to cloud particle ratios, thus, a change to riming, contact freezing, and aggregation. In the decaying stage Hector shows a wide variety of aerosol to cloud particle ratios, and the cloud particles have a simpler morphology than the particles in the mature stage, which might be an effect of ageing. Due to the varying aerosol to cloud particle number ratio, these results show that the development stage of the convective cloud system has an impact on the activation ratio and thus has to be taken into account.

In the dissipating stage Hector consists of a persistent and vertically extensive cloud layer that is optically thin. This layer certainly has non negligible effects on radiation and water vapour content. The dissipating stage could act as precursor for SVC formation. The persistent cloud layer may either lead to humidification of the TTL due to evaporation of ice crystals or by growth and sedimentation lead to dehydration of the TTL. Furthermore, shear flows may transform parts of this cloud layer into SVC. Further detailed model analyses are required to provide estimations for the de-/hydrating effect. Anyway, these observations show that the dissipating stage of a deep convective system may impose some importance and hence should not be disregarded.

The data presented in this study provide a contribution to the very sparse in situ data set of TTL convective cirrus, exhibiting a development classification. Though it consists of only one case study, this work shows the variability in TTL convective cirrus microphysics with lifetime. Besides the caveats of limited data, in situ measurements as presented here, give detailed information on the cloud microphysics which ~~cannot be obtained~~ from satellite or ground based remote sensing observations.

Acknowledgements. We thank Sebastian Raupach, Christian von Glahn, and Hermann Vössing from the University of Mainz for preparation of the CIP and FSSP instruments and collection of data during the SCOUT-O3 campaign. Special thanks to the entire "Geophysica" crew and the local authorities in Darwin for their excellent collaboration during the campaign. The SCOUT-O3 project was funded by the European Commission (GOCE-CT-2004-505390) and additional financial support was provided by the Max Planck Society and the Collaborative Research Centre "The Tropospheric Ice Phase" (SFB-641). W.F. is supported by the DFG Research Fellowship "Tropical High Altitude Clouds and their Impact on Stratospheric Humidity" (FR 3325/1-1). The work was supported in part by the ARC Centre of Excellence for Climate System Science (CE110001028). S.B. is supported by the European Research Council (Seventh Framework Program) through the ERC Advanced Grant Agreement No. 321040 (EXCATRO).

The service charges for this open access publication have been covered by the Max Planck Society.

References

Allen, G., Vaughan, G., Bower, K. N., Williams, P. I., Crosier, J., Flynn, M., Connolly, P., Hamilton, J. F., Lee, J. D., Saxton, J. E., Watson, N. M., Gallagher, M., Coe, H., Allan, J., Choularton, T. W., and Lewis, A. C.: Aerosol and trace-gas measurements in the Darwin area during the wet season, J. Geophys. Res., 113, D06306, doi:10.1029/2007JD008706, 2008. 11833, 11834

Baker, M. B.: Cloud microphysics and climate, Science, 276, 1072–1078, doi:10.1126/science.276.5315.1072, 1997. 11817

Baker, M. B. and Peter, T.: Small-scale cloud processes and climate, Nature, 451, 299–300, doi:10.1038/nature06594, 2008. 11817

Baumgardner, D., Dye, J. E., Gandrud, B. W., and Knollenberg, R. G.: Interpretation of measurements made by the Forward Scattering Spectrometer Probe (FSSP-300) during the Airborne Arctic Stratospheric expedition, J. Geophys. Res.-Atmos., 97, 8035–8046, doi:10.1029/91JD02728, 1992. 11821

Borrmann, S., Solomon, S., Dye, J. E., and Luo, B. P.: The potential of cirrus clouds for heterogeneous chlorine activation, Geophys. Res. Lett., 23, 2133–2136, doi:10.1029/96GL01957, 1996. 11817

Brunner, D., Siegmund, P., May, P. T., Chappel, L., Schiller, C., Müller, R., Peter, T., Fueglistaler, S., MacKenzie, A. R., Fix, A., Schlager, H., Allen, G., Fjaeraa, A. M., Streibel, M., and Harris, N. R. P.: The SCOUT-O3 Darwin Aircraft Campaign: rationale and meteorology, Atmos. Chem. Phys., 9, 93–117, doi:10.5194/acp-9-93-2009, 2009. 11818, 11820, 11821

Buontempo, C., Cairo, F., Di Donfrancesco, G., Morbidini, R., Viterbini, M., and Adriani, A.: Optical measurements of atmospheric particles from airborne platforms: in situ and remote sensing instruments for balloons and aircrafts, Ann. Geophys.-Italy, 49, 57–64, doi:10.4401/ag-3149, 2006. 11822

Cairo, F., Adriani, A., Viterbini, M., Di Donfrancesco, G., Mitev, V., Matthey, R., Bastiano, M., Redaelli, G., Dragani, R., Ferretti, R., Rizi, V., Paolucci, T., Bernardini, L., Cacciani, M., Pace, G., and Fiocco, G.: Polar stratospheric clouds observed during the Airborne Polar Experiment – Geophysica Aircraft in Antarctica (APE-GAIA) campaign, J. Geophys. Res., 109, D07204, doi:10.1029/2003JD003930, 2004. 11822

Cairo, F., Di Donfrancesco, G., Snels, M., Fierli, F., Viterbini, M., Borrmann, S., and Frey, W.: A comparison of light backscattering and particle size distribution measurements in tropical cirrus clouds, Atmos. Meas. Tech., 4, 557–570, doi:10.5194/amt-4-557-2011, 2011. 11821

Carbone, R. E., Wilson, J. W., Keenan, T. D., and Hacker, J. M.: Tropical island convection in the absence of significant topography. Part I: Life cycle of diurnally forced convection, Mon. Weather Rev., 128, 3459–3480, doi:10.1175/1520-0493(2000)128<3459:TICITA>2.0.CO;2, 2000. 11818, 11820, 11829

Cetrone, J. and Houze, R. A.: Anvil clouds of tropical mesoscale convective systems in monsoon regions, Q. J. Roy. Meteor. Soc., 135, 305–317, doi:10.1002/qj.389, 2009. 11828

Chemel, C., Russo, M. R., Pyle, J. A., Sokhi, R. S., and Schiller, C.: Quantifying the imprint of a severe Hector thunderstorm during ACTIVE/SCOUT-O3 onto the water content in the upper troposphere/lower stratosphere, Mon. Weather Rev., 137, 2493–2514, doi:10.1175/2008MWR2666.1, 2009. 11819, 11823

Connolly, P. J., Vaughan, G., May, P. T., Chemel, C., Allen, G., Choularton, T. W., Gallagher, M. W., Bower, K. N., Crosier, J., and Dearden, C.: Can aerosols influence deep tropical convection? Aerosol indirect effects in the Hector island thunderstorm, Q. J. Roy. Meteor. Soc., 139, 2190–2208, doi:10.1002/qj.2083, 2013. 11819, 11833

Corti, T., Luo, B. P., Fu, Q., Vömel, H., and Peter, T.: The impact of cirrus clouds on tropical troposphere-to-stratosphere transport, Atmos. Chem. Phys., 6, 2539–2547, doi:10.5194/acp-6-2539-2006, 2006. 11819

Corti, T., Luo, B. P., de Reus, M., Brunner, D., Cairo, F., Mahoney, M. J., Martucci, G., Matthey, R., Mitev, V., dos Santos, F. H., Schiller, C., Shur, G., Sitnikov, N. M., Spelten, N., Vössing, H. J., Borrmann, S., and Peter, T.: Unprecedented evidence for deep convection hydrating the tropical stratosphere, Geophys. Res. Lett., 35, L10810, doi:10.1029/2008GL033641, 2008. 11817, 11823, 11826, 11829

Curtius, J., Weigel, R., Vössing, H.-J., Wernli, H., Werner, A., Volk, C.-M., Konopka, P., Krebsbach, M., Schiller, C., Roiger, A., Schlager, H., Dreiling, V., and Borrmann, S.: Observations of meteoric material and implications for aerosol nucleation in the winter Arctic lower stratosphere derived from in situ particle measurements, Atmos. Chem. Phys., 5, 3053–3069, doi:10.5194/acp-5-3053-2005, 2005. 11822

Davis, S., Hlavka, D., Jensen, E., Rosenlof, K., Yang, Q., Schmidt, S., Borrmann, S., Frey, W., Lawson, P., Vömel, H., and Bui, T. P.: In situ and lidar observations of tropopause subvisible cirrus clouds during TC4, J. Geophys. Res., 115, D00J17, doi:10.1029/2009JD013093, 2010. 11817, 11819, 11829

de Reus, M., Borrmann, S., Bansemer, A., Heymsfield, A. J., Weigel, R., Schiller, C., Mitev, V., Frey, W., Kunkel, D., Kürten, A., Curtius, J., Sitnikov, N. M., Ulanovsky, A., and Ravegnani, F.: Evidence for ice particles in the tropical stratosphere from in-situ measurements, Atmos. Chem. Phys., 9, 6775–6792, doi:10.5194/acp-9-6775-2009, 2009. 11817, 11818, 11821, 11823, 11826, 11827, 11829, 11834

Field, P. R., Heymsfield, A. J., and Bansemer, A.: Shattering and Particle Interarrival Times Measured by Optical Array Probes in Ice Clouds, J. Atmos. Ocean. Tech., 23, 1357–1371, doi:10.1175/JTECH1922.1, 2006. 11821

Frey, W., Borrmann, S., Kunkel, D., Weigel, R., de Reus, M., Schlager, H., Roiger, A., Voigt, C., Hoor, P., Curtius, J., Krämer, M., Schiller, C., Volk, C. M., Homan, C. D., Fierli, F., Di Donfrancesco, G., Ulanovsky, A., Ravegnani, F., Sitnikov, N. M., Viciani, S., D'Amato, F., Shur, G. N., Belyaev, G. V., Law, K. S., and Cairo, F.: In situ measurements of tropical cloud properties in the West African Monsoon: upper tropospheric ice clouds, Mesoscale Convective System outflow, and subvisual cirrus, Atmos. Chem. Phys., 11, 5569–5590, doi:10.5194/acp-11-5569-2011, 2011. 11818, 11821, 11822, 11827, 11828, 11829

Fueglistaler, S., Dessler, A. E., Dunkerton, T. J., Folkins, I., Fu, Q., and Mote, P. W.: Tropical tropopause layer, Rev. Geophys., 47, RG1004, doi:10.1029/2008RG000267, 2009. 11817, 11818

Hallett, J. and Mossop, S. C.: Production of secondary ice particles during riming process, Nature, 249, 26–28, doi:10.1038/249026a0, 1974. 11832

Heymsfield, A. J., Miloshevich, L. M., Schmitt, C., Bansemer, A., Twohy, C., Poellot, M. R., Fridlind, A., and Gerber, H.: Homogeneous ice nucleation in subtropical and tropical convection and its influence on cirrus anvil microphysics, J. Atmos. Sci., 62, 41–64, doi:10.1175/JAS-3360.1, 2005. 11830, 11833

Heymsfield, A. J., Bansemer, A., Heymsfield, G., and Fierro, A. O.: Microphysics of maritime tropical convective updrafts at temperatures from −20 degrees to −60 degrees C, J. Atmos. Sci., 66, 3530–3562, doi:10.1175/2009JAS3107.1, 2009. 11830

Jensen, E. J., Toon, O. B., Selkirk, H. B., Spinhirne, J. D., and Schoeberl, M. R.: On the formation and persistence of subvisible cirrus clouds near the tropical tropopause, J. Geophys. Res., 101, 21361–21375, doi:10.1029/95JD03575, 1996. 11819, 11829

Jensen, E. J., Pfister, L., Bui, T. V., Lawson, P., Baker, B., Mo, Q., Baumgardner, D., Weinstock, E. M., Smith, J. B., Moyer, E. J., Hanisco, T. F., Sayres, D. S., Clair, J. M. St., Alexander, M. J., Toon, O. B., and Smith, J. A.: Formation of large ($\simeq 100\,\mu$m) ice crystals near the tropical tropopause, Atmos. Chem. Phys., 8, 1621–1633, doi:10.5194/acp-8-1621-2008, 2008. 11817

Jensen, E. J., Diskin, G., Lawson, R. P., Lance, S., Bui, T. P., Hlavka, D., McGill, M., Pfister, L., Toon, O. B., and Gao, R.: Ice nucleation and dehydration in the Tropical Tropopause Layer, P. Natl. Acad. Sci. USA, 110, 2041–2046, doi:10.1073/pnas.1217104110, 2013. 11819

Keenan, T. D., Ferrier, B., and Simpson, J.: Development and structure of a maritime continent thunderstorm, Meteorol. Atmos. Phys., 53, 185–222, doi:10.1007/BF01029612, 1994. 11818, 11833

Khaykin, S., Pommereau, J.-P., Korshunov, L., Yushkov, V., Nielsen, J., Larsen, N., Christensen, T., Garnier, A., Lukyanov, A., and Williams, E.: Hydration of the lower stratosphere by ice crystal geysers over land convective systems, Atmos. Chem. Phys., 9, 2275–2287, doi:10.5194/acp-9-2275-2009, 2009. 11822

Koren, I., Remer, L. A., Kaufman, Y. J., Rudich, Y., and Martins, J. V.: On the twilight zone between clouds and aerosols, Geophys. Res. Lett., 34, L08805, doi:10.1029/2007GL029253, 2007. 11820

Krüger, K., Tegtmeier, S., and Rex, M.: Variability of residence time in the Tropical Tropopause Layer during Northern Hemisphere winter, Atmos. Chem. Phys., 9, 6717–6725, doi:10.5194/acp-9-6717-2009, 2009. 11818

Lynch, D. K.: Cirrus, Oxford University Press, Oxford, Cambridge, New York, 2002. 11817

Massie, S., Gettelman, A., Randel, W., and Baumgardner, D.: Distribution of tropical cirrus in relation to convection, J. Geophys. Res.-Atmos., 107, 4591, doi:10.1029/2001JD001293, 2002. 11819

McFarquhar, G. M. and Heymsfield, A. J.: Parameterization of tropical cirrus ice crystal size distributions and implications for radiative transfer: results from CEPEX, J. Atmos. Sci., 54, 2187–2200, doi:10.1175/1520-0469(1997)054<2187:POTCIC>2.0.CO;2, 1997. 11818, 11834

Mekonnen, A., Thorncroft, C. D., and Aiyyer, A. R.: Analysis of convection and its association with African easterly waves, J. Climate, 19, 5405–5421, doi:10.1175/JCLI3920.1, 2006. 11828

Mitev, V., Matthey, R., and Makanov, V.: Miniature backscatter lidar for cloud and aerosol observation from high altitude aircraft, Rec. Res. Dev. Geophys, 4, 207–223, doi:10.1127/0941-2948/2005/0046, 2002. 11822

Park, S., Jiménez, R., Daube, B. C., Pfister, L., Conway, T. J., Gottlieb, E. W., Chow, V. Y., Curran, D. J., Matross, D. M., Bright, A., Atlas, E. L., Bui, T. P., Gao, R.-S., Twohy, C. H., and Wofsy, S. C.: The CO_2 tracer clock for the Tropical Tropopause Layer, Atmos. Chem. Phys., 7, 3989–4000, doi:10.5194/acp-7-3989-2007, 2007. 11818

Rosenfield, J. E., Considine, D. B., Schoeberl, M. R., and Browell, E. V.: The impact of subvisible cirrus clouds near the tropical tropopause on stratospheric water vapor, Geophys. Res. Lett., 25, 1883–1886, doi:10.1029/98GL01294, 1998. 11819

Saito, K., Keenan, T., Holland, G., and Puri, K.: Numerical simulation of the diurnal evolution of tropical island convection over the Maritime Continent, Mon. Weather Rev., 129, 378–400, doi:10.1175/1520-0493(2001)129<0378:NSOTDE>2.0.CO;2, 2001. 11818, 11819

Shur, G., Sitnikov, N., and Drynkov, A.: A mesoscale structure of meteorological fields in the tropopause layer and in the lower stratosphere over the southern tropics (Brazil), Russ. Meteorol. Hydrol., 32, 487–494, doi:10.3103/S106837390708002X, 2007. 11822

Sitnikov, N. M., Yushkov, V. A., Afchine, A. A., Korshunov, L. I., Astakhov, V. I., Ulanovskii, A. E., Krämer, M., Mangold, A., Schiller, C., and Ravegnani, F.: The FLASH instrument for water

vapor measurements on board the high-altitude airplane, Instrum. Exp. Tech., 50, 113–121, doi:10.1134/S0020441207010174, 2007. 11822

Sokolov, L. and Lepuchov, B.: Protocol of Interaction Between Unit for Connection with Scientific Equipment (UCSE) and On-Board Scientific Equipment of Geophysica Aircraft (Second edition), Myasishchev Design Bureau (MDB), Moscow, Russia, 1998. 11822

Solomon, S., Borrmann, S., Garcia, R. R., Portmann, R., Thomason, L., Poole, L. R., Winker, D., and McCormick, M. P.: Heterogeneous chlorine chemistry in the tropopause region, J. Geophys. Res.-Atmos., 102, 21411–21429, doi:10.1029/97JD01525, 1997. 11817

Solomon, S., Thompson, D. W. J., Portmann, R. W., Oltmans, S. J., and Thompson, A. M.: On the distribution and variability of ozone in the tropical upper troposphere: implications for tropical deep convection and chemical-dynamical coupling, Geophys. Res. Lett., 32, L23813, doi:10.1029/2005GL024323, 2005. 11825

Stith, J. L., Haggerty, J. A., Heymsfield, A., and Grainger, C. A.: Microphysical characteristics of tropical updrafts in clean conditions, J. Appl. Meteorol., 43, 779–794, doi:10.1175/2104.1, 2004. 11831

Thompson, A., Tao, W., Pickering, K., Scala, J., and Simpson, J.: Tropical deep convection and ozone formation, B. Am. Meteorol. Soc., 78, 1043–1054, doi:10.1175/1520-0477(1997)078<1043:TDCAOF>2.0.CO;2, 1997. 11825

Ulanovsky, A. E., Yushkov, V. A., Sitnikov, N. M., and Ravegnani, F.: The FOZAN-II fast-response chemiluminescent airborne ozone analyzer, Instrum. Exp. Tech., 44, 249–256, doi:10.1023/A:1017535608026, 2001. 11823

von Hobe, M., Grooß, J.-U., Günther, G., Konopka, P., Gensch, I., Krämer, M., Spelten, N., Afchine, A., Schiller, C., Ulanovsky, A., Sitnikov, N., Shur, G., Yushkov, V., Ravegnani, F., Cairo, F., Roiger, A., Voigt, C., Schlager, H., Weigel, R., Frey, W., Borrmann, S., Müller, R., and Stroh, F.: Evidence for heterogeneous chlorine activation in the tropical UTLS, Atmos. Chem. Phys., 11, 241–256, doi:10.5194/acp-11-241-2011, 2011. 11817

Weigel, R., Hermann, M., Curtius, J., Voigt, C., Walter, S., Böttger, T., Lepukhov, B., Belyaev, G., and Borrmann, S.: Experimental characterization of the COndensation PArticle counting System for high altitude aircraft-borne application, Atmos. Meas. Tech., 2, 243–258, doi:10.5194/amt-2-243-2009, 2009. 11822

Weigel, R., Borrmann, S., Kazil, J., Minikin, A., Stohl, A., Wilson, J. C., Reeves, J. M., Kunkel, D., de Reus, M., Frey, W., Lovejoy, E. R., Volk, C. M., Viciani, S., D'Amato, F., Schiller, C., Peter, T., Schlager, H., Cairo, F., Law, K. S., Shur, G. N., Belyaev, G. V., and Curtius, J.: In situ

observations of new particle formation in the tropical upper troposphere: the role of clouds and the nucleation mechanism, Atmos. Chem. Phys., 11, 9983–10010, doi:10.5194/acp-11-9983-2011, 2011. 11818, 11831

Winker, D. M. and Trepte, C. R.: Laminar cirrus observed near the tropical tropopause by LITE, Geophys. Res. Lett., 25, 3351–3354, doi:10.1029/98GL01292, 1998. 11817, 11819

Yushkov, V., Oulanovsky, A., Lechenuk, N., Roudakov, I., Arshinov, K., Tikhonov, F., Stefanutti, L., Ravegnani, F., Bonafe, U., and Georgiadis, T.: A chemiluminescent analyzer for stratospheric measurements of the ozone concentration (FOZAN), J. Atmos. Ocean. Tech., 16, 1345–1350, doi:10.1175/1520-0426(1999)016<1345:ACAFSM>2.0.CO;2, 1999. 11823

Table 1. Averages of microphysical and meteorological properties for the different Hector stages and altitude bins as in Fig. 6. That is: ice water content (IWC), cloud particle number concentration (N), effective radius (r_{eff}), relative humidity with respect to ice (RHi), and ambient temperature (T). The last column indicates the number of size distributions (#) for each class.

$T_{\text{potential}}$ [K]	case	IWC [10^{-3} g m^{-3}]	N [cm^{-3}]	r_{eff} [µm]	RHi [%]	T [K]	#
350–355	dev	0.21	0.02	21.8	–	199.3	1
	mat	4.44	0.30	74.5	83	200.4	6
	dis	2.78	0.20	36.6	72*	205.6	6
355–360	dev	0.21	0.03	16.8	–	195.0	27
	mat	4.73	0.44	41.6	95	195.1	19
	dis	0.27	0.14	14.9	105	195.5	10
360–365	dev	0.04	0.02	9.1	–	189.2	3
	mat	3.12	0.45	14.9	100	189.7	4
	dis	0.08	0.05	10.2	91	192.0	100
365–370	dev	0.03	0.06	5.7	–	186.9	2
	mat	0.16	0.07	14.1	105	188.7	5
	dis	0.03	0.02	8.6	110	187.2	1
370–375	dev	0.002	0.007	3.2	–	186.0	1
	mat	0.016	0.009	5.9	113	187.6	3
	dis	0.008	0.008	5.1	101	188.1	3

* RHi measurements only available for 5 size distributions.

Table 2. Averages of activation ratio estimate and aerosol number concentrations for the different Hector stages and altitude bins as in Fig. 6. Note that aerosol measurements are not available for all given size distributions.

$T_{\text{potential}}$ [K]	case	activation ratio $\times 10^{-4}$	N_{aerosol} [cm^{-3}]
350–355	dev	1.05	191
	mat	20.29	238
	dis	no N_{aerosol}	no N_{aerosol}
355–360	dev	1.24	233
	mat	11.99	226
	dis	8.22	199
360–365	dev	1.26	182
	mat	30.15	151
	dis	2.35	248
365–370	dev	3.91	144
	mat	4.99	130
	dis	1.61	110
370–375	dev	0.55	123
	mat	1.03	93
	dis	0.97	88

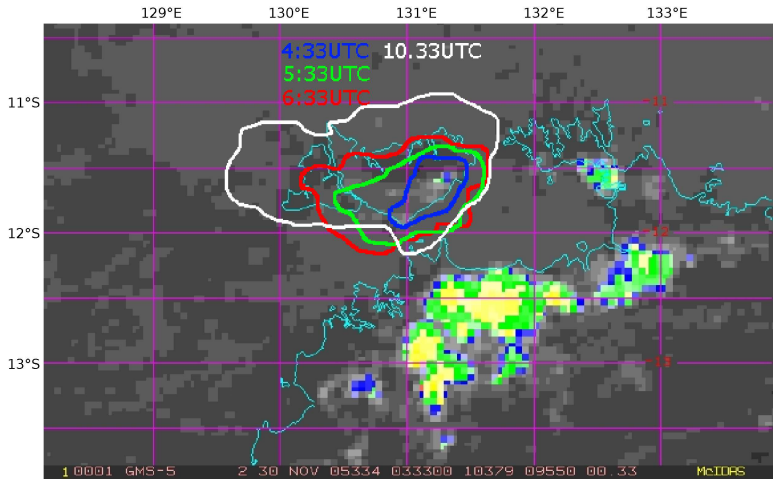

Fig. 1. GMS infra-red (IR) cloud top temperature satellite image of the Tiwi Island region. First cloud patches of the developing Hector can be seen. The evolution of Hector is depicted with the coloured contours (see text for explanation). The satellite cloud top temperature colour scale is: > 250 K grey shades, 250–230 K blue shades, 230–210 K green shades, 210–190 K yellow shades, < 190 K red shades.

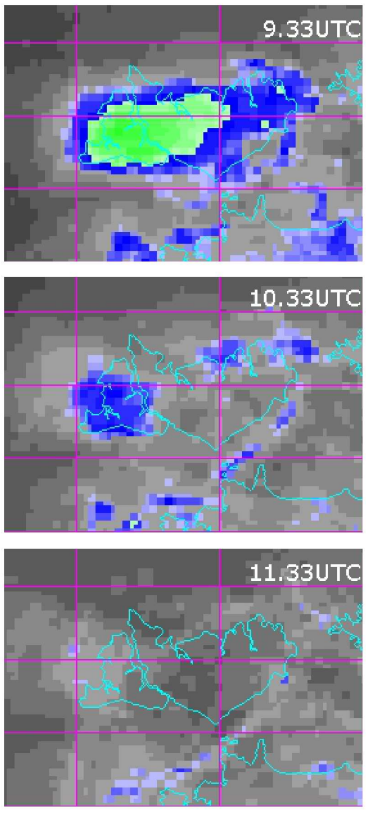

Fig. 2. Close-up of GMS IR satellite images of the Tiwi Island region. The ~~dissolving~~ Hector can be seen. The colour scale is as in Fig. 1.

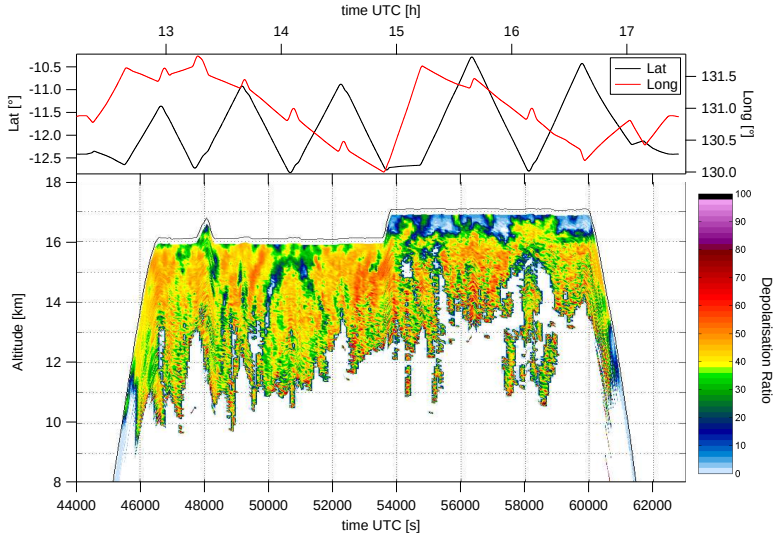

Fig. 3. Depolarisation ratio measured by the downward looking lidar MAL during the second flight. The remnants of Hector can clearly be seen. The top panel indicates the aircrafts position (latitude and longitude). The lidar sees a surface return at all times (not shown here), thus, the cloud layer thickness should be completely captured and well represented. A figure for the first flight is omitted since it is not possible to say whether the layer thickness is adequately presented at all times, due to thick clouds and the laser beam not being able to penetrate through the entire cloud vertical extent. The cloud tops, if not overshooting, were roughly located at about 17 km during the first flight.

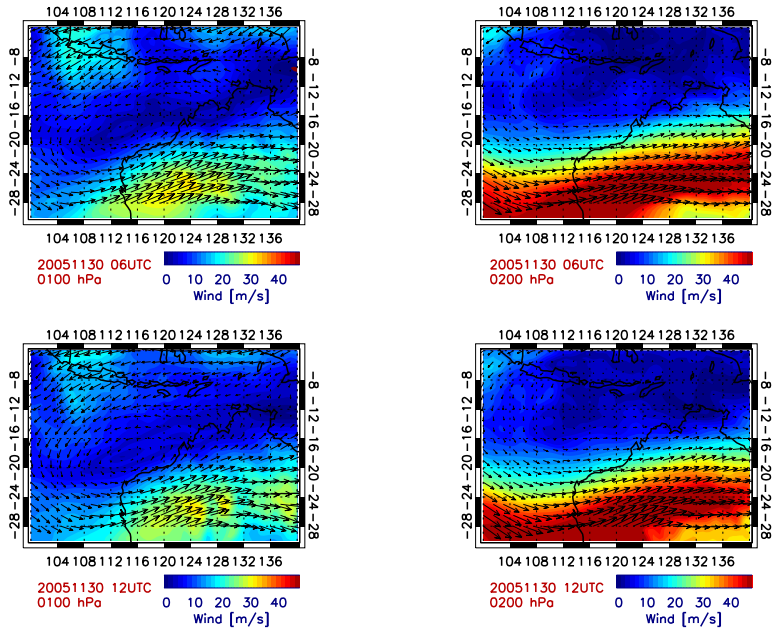

Fig. 4. Wind fields from ECMWF at 100 hPa (left panels) and 200 hPa (right panels) at 06:00 UTC (upper panels) and 12:00 UTC (lower panels).

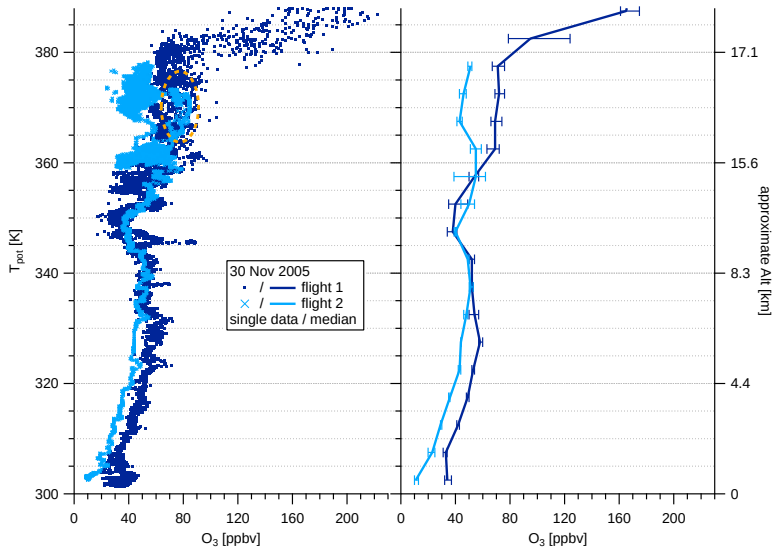

Fig. 5. Profiles of ozone mixing ratios from first and second flight on 30 November 2005. Individual (1 Hz) data points are shown in the left panel, median and 33/67 percentiles in the right panel. The orange ellipse encloses data points that were recorded at the beginning of the second flight at the eastern edge of the flight path. The number of these points are much lower than those at later times of the flight, thus, these observations have no visible effect on the median as shown in the right panel.

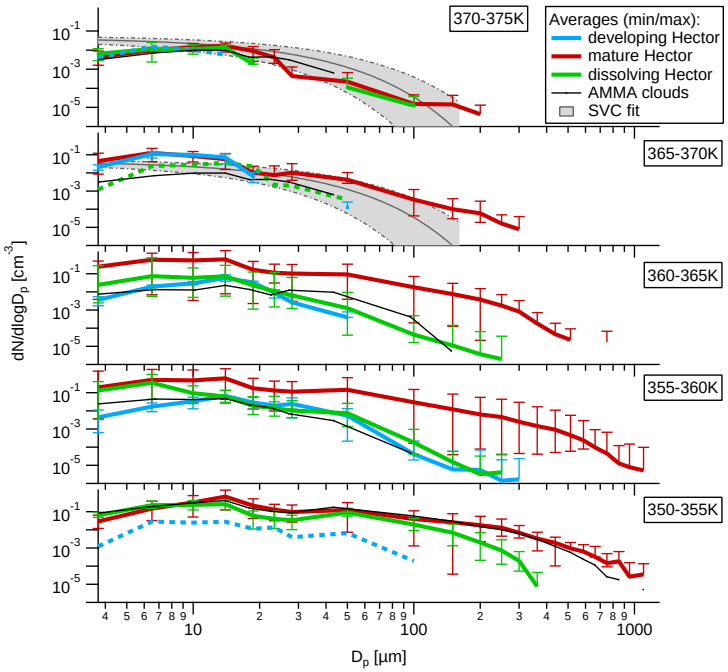

Fig. 6. Vertical profile of size distributions. The averages of the respective Hector development stage (developing, mature, and dissolving) for every potential temperature bin of 5 K are given. A dashed line denotes that only one size distribution for the respective Hector class had been measured in the respective altitude bin. Vertical bars show the position of the minimum and maximum distribution for the respective average. Further parameters can be found in Table 1 Additionally, the mean size distributions of measurements inside MCS anvil outflow during AMMA and a fit for subvisible cirrus are displayed.

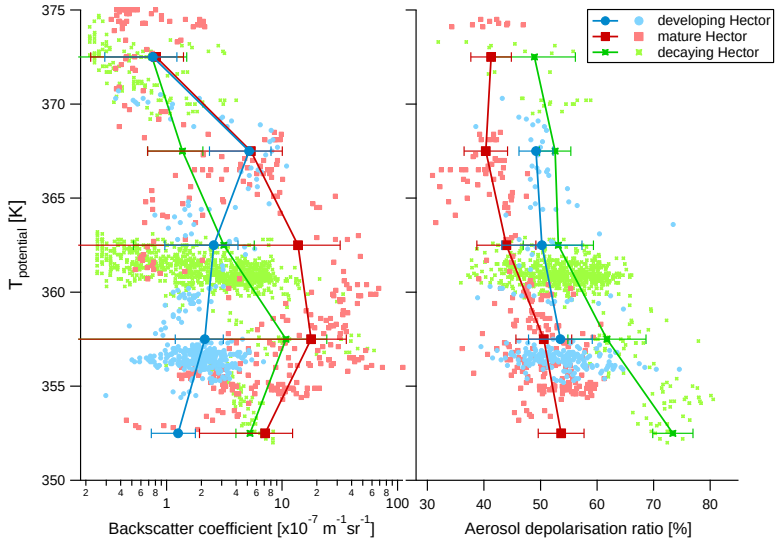

Fig. 7. MAS aerosol backscatter coefficient (left) and aerosol depolarisation ratio (right). The light coloured markers indicate the individual measurements. Lines and markers represent the averages for the 5 K altitude bins as in Fig. 6 with error bars denoting the standard deviation.

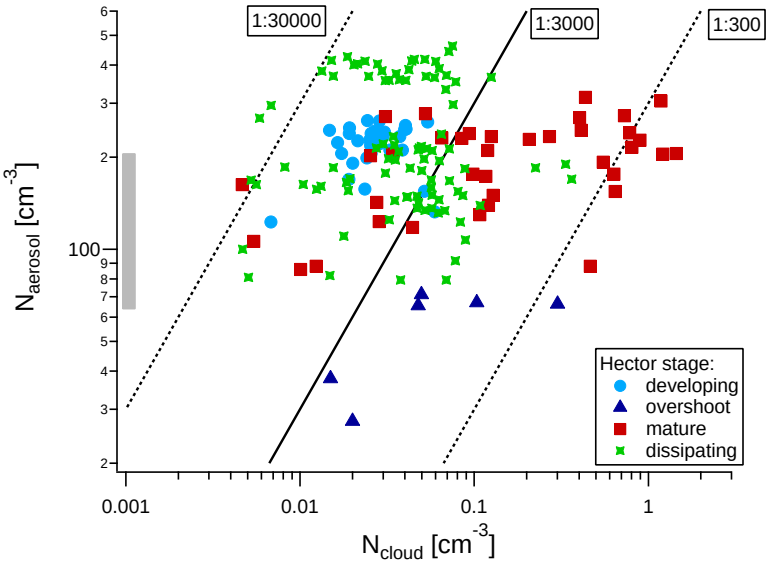

Fig. 8. Activation of aerosol to cloud particles estimated by the number concentrations of aerosol and cloud particles. The points correspond each to one size distribution in Fig. 6, with the same colour code. The overshooting Hector cases were observed at potential temperatures of 386–414 K. The grey bar on the left denotes in-cloud aerosol concentrations observed on other flights during SCOUT-O3. See text for further explanation.

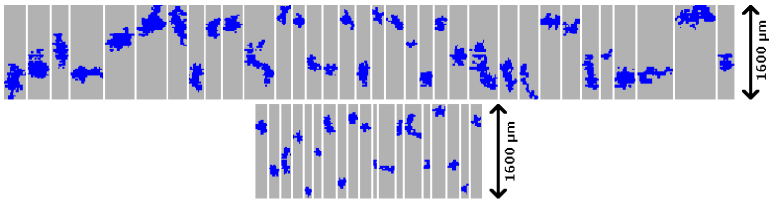

Fig. 9. Images taken by the CIP during the mature (upper) and dissipating (lower panel) Hector phase. No developing Hector images are shown since these were only a few pixels and no shapes can be inferred from these images.